Balanced Comparator for RSFQ Qubit Readout

Tom Ohki, Alexander Savin, Juha Hassel, Leif Grönberg, Tatiana Karminskaya, and Anna Kidiyarova-Shevchenko

***Abstract*—The balanced comparator is an essential part of RSFQ-based readout for superconducting qubits. In this paper we report measurements of the sensitivity of the balanced comparator fabricated in a specialized 30 $\mathrm{A/cm^2}$ process with 3.6 μA critical currents and measured at 30–500 mK. At sampling frequency of 3.5 GHz the measured gray zone is $\Delta I = 104$ nA. Due to electron overheating in the shunt resistors the effective noise temperature is 140 mK. The gray zone has a strong dependence on sampling frequency above 5 GHz due to over-clocking. Related measurements have been reported where cooling fins and reduced critical current density of 10 $\mathrm{A/cm^2}$ were used, and a quantum limited gray zone of *40 nA* was achieved. This makes single shot readout possible for the phase, RF-SQUID and persistent current qubits. The readout speed is 30-50 ps, which is quite favorable for error correction schemes.**

***Index Terms*—Balanced comparator, qubit readout, RSFQ.**

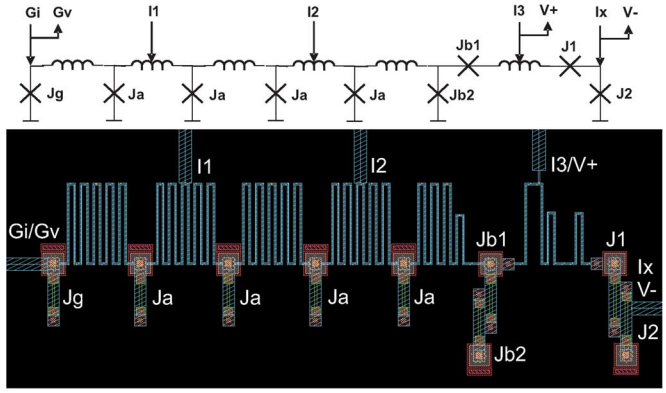

Fig. 1. Test circuit for measurement of the balanced comparator sensitivity: schematic and mask layout using the VTT 30 $\mathrm{A/cm^2}$ process.

I. Introduction

QUANTUM computing cannot be implemented using qubits alone. Classical electronics plays an important role particularly for error correction. Quantum error correction protects information encoded in qubits by restoring states based on certain conditional measurements. Error correction involves measurement, logic processing and control operations that must be completed quickly, on the time scale of the quantum gate operations [1].

For superconducting qubits the only classical electronics candidate that fits is RSFQ superconducting digital technology [2], which performs the required logic functions on a time scale of 10 ps and can be integrated with the qubits at mK [3], [4]. The main challenge with this technology is reaching the required readout sensitivity without introducing decoherence from dissipative shunts used in RSFQ circuits.

Two basic strategies for building an RSFQ based readout have been proposed in the literature. The first uses time-delay detection of ballistic fluxons propagated in the vicinity of the qubit [5]. The second uses detection of either current or magnetic flux using the balanced comparator triggered by SFQ pulses [6], [7].

Manuscript received August 27, 2006. This work was supported in part by EU FP6 grant "RSFQubit," SSF "INGVAR" grant, VR grant N2003-10990-17764-11, and STINT "Gigahertz electronics" grant. A. Kidiyarova-Shevchenko is supported by The Royal Swedish Academy of Sciences by a grant from the Knut and Alice Wallenberg Foundation.

T. Ohki and A. Kidiyarova-Shevchenko are with Microtechnology and Nanoscience Dept., Chalmers University of Technology, 41296 Gothenburg, Sweden (e-mail: Anna.Kidiyarova-Shevchenko@mc2.chalmers.se).

A. Savin is with Helsinki University of Technology, Finland.

J. Hassel and L. Grönberg are with VTT, Finland.

T. Karminskaya is with Moscow State University, Nuclear Physics Institute, Russia.

Color versions of one or more of the figures in this paper are available online at http://ieeexplore.ieee.org.

Digital Object Identifier 10.1109/TASC.2007.897319

SFQ comparators have been well-characterized and have been proven to be good current sensors [8], [9]. In this paper we report measurements of the balanced comparator designed to operate at milli-Kelvin temperatures. Based on comparison with related measurements performed at Helsinki University of Technology [10] we explore techniques to reach quantum-limited operation and ideal noise characteristics of the comparator. The final numbers are discussed in the context of single shot readout for superconducting flux, phase and charge-phase qubits.

II. Test Circuit

The test circuit for measurements of comparator sensitivity is shown in Fig. 1. It consists of a generator junction J_g, a Josephson transmission line with four junctions J_a, a buffer stage J_{b1} and J_{b2}, and a comparator J_1 and J_2.

The operating principal of the circuit has been reported previously [8]. A brief description of the circuit function is as follows. The generator junction is current biased such that a train of SFQ pulses with frequency f is produced following the relationship

$$\langle V \rangle = f\Phi_0, \tag{1}$$

where $\langle V \rangle$ is the average voltage across junction, and $\Phi_0 = h/2e$. The pulses propagate down the transmission line and switch one of the comparator junctions depending on the sign of the current I_x. The measured voltage across the comparator junction J_2 is a step function equal to zero at negative I_x and equal to the generator voltage at positive I_x. Near threshold, noise introduces broadening of the step function. The result is the error function, whose characteristic width, or "gray zone," is ΔI. The derivative of the error function is the normal distribution, and so the gray zone width can be related to the standard deviation, σ, by $\Delta I = \sigma\sqrt{2\pi}$.

In the thermal limit, the gray zone scales as the square root of critical current and temperature.

$$\Delta I \approx \alpha(2\pi I_T I_C)^{1/2}, \tag{2}$$

where $I_T = 2e/\hbar(k_B T)$ is the thermal current. The dimensionless parameter α includes the dependence on the initial phase set by comparator bias current, I3, and the rate $d\phi/dt$ of the sampling SFQ pulse.

At low temperatures there exists a transition from thermal to quantum-limited measurements. In the quantum limit the gray zone, I_Q, exhibits similar behavior in relation to critical current [9] with a natural scale $I_Q = 2e/\hbar(\hbar\omega_p)$, where ω_p is the Josephson plasma frequency. The crossover temperature for Josephson junctions with dissipation can be estimated as [11]:

$$T^* = \frac{\hbar\omega_p}{2\pi k_B}\left[\left(1+\frac{1}{4\beta_c}\right)^{1/2} - \frac{1}{2}\left(\frac{1}{\beta_c}\right)^{1/2}\right]. \tag{3}$$

In practice, the quantum-limited regime is very difficult to achieve due to electron overheating in shunt resistors of the junctions. At mK temperatures, the electron temperature T_e depends on phonon temperature T_p and applied power, P, in accordance with a "fifth-power" law [12]:

$$T_e = \left(P/\Sigma\Lambda + T_p^5\right)^{1/5}, \tag{4}$$

where Σ is a material constant and Λ is the resistor volume. For conventional RSFQ circuits operated at a bath temperature below 100 mK, measured electron temperature saturates at about 500 mK [4].

III. Circuit Design and Parameters

The circuit shown in Fig. 1 was designed for the VTT 30 $\mathrm{A/cm^2}$ process [13]. The junctions have a NbAlOxNb trilayer with Pd shunt resistors. The circuit has small critical currents and no bias resistors in order to meet the small thermal budget at mK temperatures [3].

Parameter values of the comparator were estimated using the IV characteristics of the junctions, measured individually at 4.2 K. The experimental data were fitted with theoretical curves obtained by solving the Langevin equation including a fluctuation term (Fig. 2). The measured parameters of the comparator along with designed values, calculated β_c and T^* are summarized in Table I. The measured critical current of 3.6 μA is 15% less than the designed value, which is within the fabrication spread. The deviation can be attributed to a decrease in either junction area or critical current density. These two cases lead to a possible deviation in T^* of 4 mK.

The remainder of the circuit has the following parameters: $J_a = J_g = 3.6$ μA, $J_{b1} = 2.13$ μA, $J_{b2} = 3.1$ μA. All junctions have $\beta_c = 0.59$ except the generator junction with $\beta_c = 0.47$. The circuit parameters were chosen such that power is evenly distributed to avoid hot spots. The circuit inductors have normalized values equal to $\Phi_0/2\pi I_c/2$.

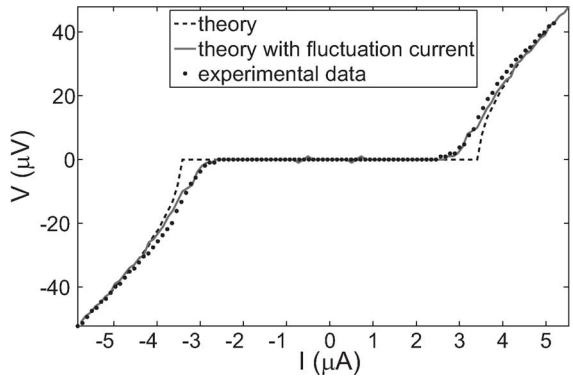

Fig. 2. IV characteristics of the comparator junction J_1. Measured data at 4.2 K and theoretical fit.

TABLE I
Designed and Measured Parameters of the Balanced Comparator

	I_c (μA)	R_N (Ω)	$I_c R_N$ (μV)	β_c	T^* (mK)
Design	4.24	15	63.6	1.84	114
Experiment	3.6	10	36	0.59	89

IV. Experiment

A. Measurement Setup

The measurements were performed at Helsinki University of Technology in an He3-He4 dilution refrigerator with a base temperature of 30 mK. Signal filtering is accomplished via thermocoax from 1.5 K down to the mK stage, and 1 MHz low-pass filters at room temperature. The noise floor of the setup is lower than 10 nA. There is an approximately 500 Ω lead-resistance at stages below 1.5 K so heating from bias currents is an issue. We applied currents up to 5.4 μA and achieved base temperatures of 50–65 mK.

B. Probability Distribution

To measure the switching probability, the signal current I_x was ramped around zero bias and the resulting error function of the voltage across J_2 was recorded (Fig. (3a)). In order to obtain the probability distribution, I_x was modulated at 8 Hz and a lock-in amplifier was used to measure dV/dI of the voltage response. The derivative of the voltage step that characterizes the gray zone was fitted to a Gaussian as shown in Fig. (3b). Both the switching probability (error function) and the probability distribution (normal distribution) are measured data.

The comparator bias I_3 was optimized to achieve the narrowest gray zone. Data were taken from 2-20 GHz. The probability distribution has perfect Gaussian fit with $\xi < 10^{-4}$ up to 14 GHz. Within this range the height of the voltage step was equal to the generator voltage. Above 14 GHz the circuit response exhibited signs of circuit malfunction.

C. Frequency Dependence

Fig. 4 illustrates the dependence of ΔI on the generator frequency. For 2–5 GHz an increase in ΔI is visible and follows the theory [8]. However, there is a steady decrease of ΔI from 5 GHz to 14 GHz. The 5 GHz frequency corresponds to $1/f \approx$

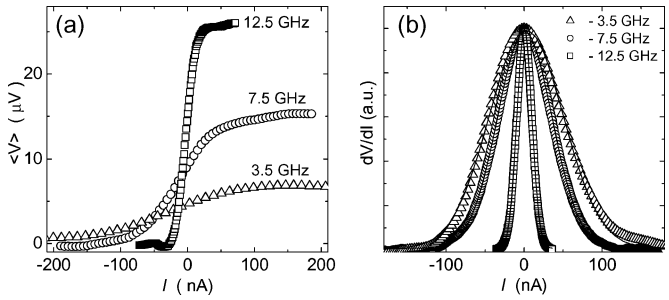

Fig. 3. (a) Switching probability and (b) probability distribution of the balanced comparator at the threshold given for different frequencies. The derivatives are normalized for clarity.

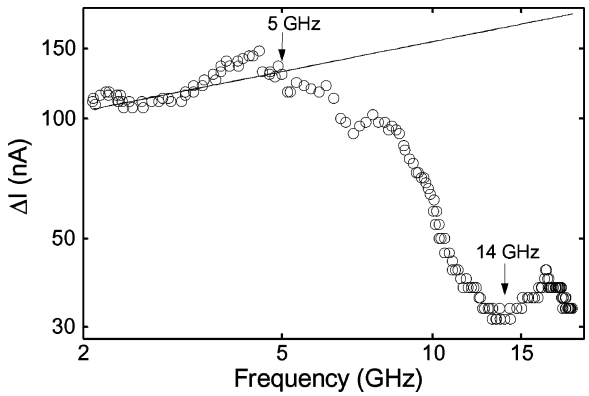

Fig. 4. Gray zone frequency dependence measured at bath temperature 30 mK.

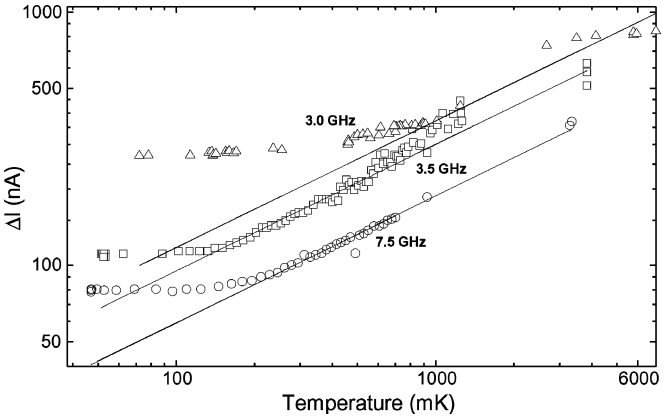

Fig. 5. Gray zone temperature dependence for two generator frequencies of 3.5 (squares) and 7.5 GHz (circles). The third set (triangles) of data is from a similar experiment recently performed at Helsinki University of Technology on the samples from the same wafer [10].

$3.5\tau = 200$ ps, where $\tau \approx 57.5$ ps is the switching time of the Josephson junction with $I_c R_N = 36\ \mu$V. Above this frequency the DC current biased comparator model [8] would be more appropriate and the circuits is no longer operating as an SFQ comparator. The steadily decreasing "gray zone" might be explained by the increasing impedance of the driver circuit.

D. Temperature Dependence

Fig. 5 shows typical temperature dependence of the gray zone given for SFQ clock frequencies of 3.5 and 7.5 GHz. The third set of data is from similar measurements recently performed by Helsinki University of Technology using samples from the same wafer [10].

It can be seen that the gray zone decreases with temperature until it saturates at some level. Measured saturation temperatures for the 3.5 and 7.5 GHz frequencies are correspondingly 160 and 190 mK. Both these temperatures are above crossover temperature T^*.

The relative increase in electron temperature with frequency perfectly scales in accordance with (4) taking into account the increased power dissipation in the junctions, $P = I_c \Phi_0 f$. However, the absolute value of electron temperature is below the theoretical prediction. For a given volume of the two closely connected shunts, $\Lambda = 3.708 * 10^{-17}\ \mathrm{m}^3$, material constant $\Sigma = 2 * 10^9\ \mathrm{W/K^5 m^3}$, and power $P = 26.08$ pW (3.5 GHz) and $P = 55.89$ pW (7.5 GHz) (4) results in electron temperatures of 177 mK and 237 mK respectively.

There are two main hypotheses for the discrepancy between theoretical prediction and measured electron temperature. First, there is possibly another channel for energy dissipation, i.e. radiation resistance of the on-chip wires between comparator circuit and contact pads. Using (4) one can estimate that the measured electron temperature can be reached if only 60% of the total power is actually dissipated in the shunts. This would imply that the other 40% is dissipated in radiative losses. The second hypothesis is that there are non-equilibrium heating effects. Equation (4) is given for DC power dissipation. This may not be valid for the SFQ pulse train in question, which has $\approx 30\%$ duty cycle.

Above the saturation point experimental data for ΔI fits well with a $\sqrt{T}$ dependence according to (2). At the saturation point, the gray zone wa 76 nA at 7.5 GHz and 103 nA at 3.5 GHz. The parameter α from (2) for 7.5 GHz and 3.5 GHz are 0.19 and 0.28 respectively. Both values correspond to the very high comparator clocking frequency.

E. Comparison With Related Experiment

The third set of data shown in Fig. 3 was obtained with a comparator having similar parameters: $J_1 = J_2 = 2.1\ \mu$A, $\beta_c = 0.5$. This results in a similar maximum operating frequency of about 6 GHz. The measured saturation temperature, $\simeq 500$ mK and gray zone $\simeq 250$ nA are higher than reported in the previous section and higher than the theoretical values. This indicates the presence of additional noise in the circuit, which we attribute to relatively poor isolation in the simplified comparator design.

Apart from the larger gray zone, the experiment in [10] yielded two important results. Measurements of the same comparator with cooling fins attached to the shunt resistors showed a fourfold decrease in electron temperature down to $\simeq$ 120–130 mK and a corresponding decrease of ΔI down to 130 nA. Measurements of the 10 $\mathrm{A/cm^2}$ sample with $I_c = 0.6\ \mu$A at 2 GHz approached the quantum limit with 30-40 mK electron temperature and current sensitivity 40 nA.

Application of the same techniques for the circuit presented in this paper would suggest quantum-limited operation with $T_e = T^* \simeq 89$ mK, $\Delta I \simeq 77.8$ nA for a 30 $\mathrm{A/cm^2}$ process, and $T_e = T^* \simeq 51$ mK, $\Delta I \simeq 26$ nA for 10, $\mathrm{A/cm^2}$ process.

TABLE II
PARAMETERS OF THE BALANCED COMPARATOR FOR QUBIT READOUT

J_c A/cm^2	T mK	I_c μA	ΔI nA	$\Delta\Phi/\Phi_0$	R_N Ω	τ ps
1000 [8]	4.2	145	6.5*10^3	3.7*10^{-3}	2	10
30 Sec. IV	160	3.6	104	2.3*10^{-3}	10	57
10 [10]	30	0.6	40	5.31*10^{-3}	15.4	100

V. APPLICATION TO QUBIT READOUT

The balanced comparator can be used for qubit readout either as a current sensor by direct coupling to the qubit or as a magnetic flux sensor by incorporating it into a SQUID loop that is inductively coupled to the qubit. The direct coupling approach is similar to the readout used for the charge-phase qubit [14], and the phase qubit [15]. These require very high current resolution of 10 and 30 nA respectively.

For the inductively coupled SQUID approach the required flux resolution depends on the type of qubit used: Φ_0 for the phase qubit [16], about 300 $\mathrm{m}\Phi_0$ for the RF-SQUID qubit [17], 10 $\mathrm{m}\Phi_0$ for the PC-qubit [18], and 10 $\mu\Phi_0$ for the charge-phase qubit [14].

In theory, sensitivity of the SQUID with the balanced comparator is given by $\Delta\Phi = \Delta I L$, where L is a SQUID loop inductance. The optimum inductance of the SQUID corresponds to one half flux quanta in the loop, $L \simeq= \Phi_0/4\pi I_c$. This means that flux sensitivity is determined by the ratio between comparator gray zone and critical current rather than by the gray zone itself:

$$\Delta\Phi = \frac{1}{2}\frac{\Phi_0}{2\pi}\frac{\Delta I}{I_c}. \tag{5}$$

Combining (2) and (5) shows that flux resolution proportional to the square root of the ratio between thermal and critical currents, $\Delta\Phi \sim \sqrt{I_T/I_c}$, and is almost constant with temperature.

Table II summarizes parameters of the balanced comparator relevant for the qubit readout reported previously [8], [10], and in the current paper.

Table II indicates that the current resolution of the balanced comparator is not adequate for direct coupling readout schemes of the charge-phase qubit, and is marginal for the phase qubit. Flux resolution is two orders of magnitude better then required for single shot measurements of the RF-SQUID qubit and is marginal for the PC-qubit.

Beyond sensitivity, the qubit readout scheme must produce low backaction, which is characterized by the circuit impedance and effective noise temperature. The impedance of the RSFQ circuit as seen by the qubit is equal to the shunt resistance, $|Z(\omega)| \approx R_N$. A shunt resistance on the order of 10 Ω or less prevents direct-coupled readout since the coupling of noise cannot be isolated effectively. Higher impedance can be reached by using a low J_c process and $\beta_c = 2$. Further reduction of the backaction can be achieved by weak coupling of the RSFQ readout to the qubit and application of a tunable transformer that eliminates first-order coupling [9].

Target parameters of the comparator for two low J_c processes and $\beta_c = 2$ are given in Table III. The sensitivity figures are given for the quantum limit, which implies use of cooling fins. For these parameters single shot readout is possible for the phase qubit with 10^{-3} coupling, the RF-SQUID qubit with 10^{-2} coupling, and the PC-qubit with 0.5 coupling coefficient. The sensitivity that is required for charge-phase qubit is beyond what is achievable in single-shot mode.

TABLE III
TARGET PARAMETERS OF THE BALANCED COMPARATOR

J_c A/cm^2	T mK	I_c μA	ΔI nA	$\Delta\Phi/\Phi_0$	R_N Ω	τ ps
30	115	3.6	87	1.92*10^{-3}	31	31
10	68	0.7	30	3.41*10^{-3}	53	54

The readout speed is equal to switching time of the comparator junctions: 31 ps for 30 $\mathrm{A/cm^2}$ process and 54 ps for 10 $\mathrm{A/cm^2}$ process. Combining fast readout and fast processing of the data on chip, RSFQ technology offers realization of the feedback required for error correction on a time scale of less than 1 ns.

ACKNOWLEDGMENT

The authors wish to thank Jukka Pekola from Helsinki University of Technology, and Chris Lobb and Fred Wellstood from University of Maryland for discussions and comments.

REFERENCES

[1] A. M. Steane, "Overhead and noise threshold of fault-tolerant quantum error corrections," *Phys. Rev. A*, vol. 68, p. 042 322-1, 2003.
[2] K. K. Likharev and V. K. Semenov, "RSFQ logic/memory family: a new Josephson-junction digital technology for sub-terahertz-clock-frequency digital systems," *IEEE Trans. On Appl. Supercond.*, vol. 1, no. 1, p. 3, 1991.
[3] S. Intiso and J. Pekola *et al.*, "Rapid single-flux-quantum circuits for low noise mK operation," *Supercond. Science and Techn.*, vol. 19, p. 335, 2006.
[4] A. M. Savin *et al.*, "Thermal budget of superconducting digital circuits at subkelvin temperatures," *Journal of Applied Physics*, vol. 99, p. 084501, 2006.
[5] D. V. Averin, K. Rabenstein, and V. K. Semenov, "Rapid ballistic readout for flux qubits," *Phys. Rev. B*, vol. 73, p. 094504, 2006.
[6] V. Semenov and D. Averin, "SFQ control circuits for Josephson junction qubits," *IEEE Trans. on Appl. Supercond.*, vol. 13, p. 960, 2003.
[7] T. A. Ohki, M. Wulf, M. J. Feldman, and M. F. Bocko, "Unshunted QOS comparator for qubit readout," *J. Phys. Conf. Ser.*, vol. 43, p. 1413, 2006.
[8] V. Semenov, T. Filippov, Y. Polyakov, and K. Likharev, "SFQ balanced comparators at a finite sampling rate," *IEEE Trans. Applied Superconductivity*, vol. 7, no. 2, p. 3617, 1997.
[9] T. Walls *et al.*, "Quantum fluctuations in Josephson junction comparators," *Phys. Rev. Lett.*, vol. 89, p. 217004, 2002.
[10] A. Savin and J. Pekola *et al.*, "High resolution superconducting single flux quantum comparator for sub Kelvin temperatures," *Appl. Phys. Lett.*, vol. 89, p. 133505, 2006.
[11] H. Grabert, P. Olschowski, and U. Weiss, "Quantum decay rates for dissipative systems at finite temperatures," *Physical Review B*, vol. 36, no. 4, p. 1931, 1987.
[12] F. Wellstood, C. Urbina, and J. Clarke, "Hot electron effects in metals," *Physical Review B*, vol. 49, no. 9, p. 5942, 1994.
[13] L. Gronberg and J. Hassel *et al.*, "Characterization of a fabrication process for the integration of superconducting qubits and RSFQ circuits," *Supercond. Sci. Technol.*, vol. 19, p. 860, 2006.
[14] D. Vion, A. Assime, and A. Cottet *et al.*, "Manipulating the quantum state of an electrical circuit," *Science*, vol. 296, no. 886, p. 886, 2003.
[15] T. A. Palomaki, S. K. Dutta, and R. M. Lewis *et al.*, Fast High-Fidelity Measurements of the Ground and Excited States of a dc SQUID Phase Qubit 2006, ArXiv:cond-mat/0608399.
[16] N. Katz, M. Ansmann, and R. C. Bialczak *et al.*, "Coherent state evolution in a superconducting qubit from partial-collapse measurement," *Science*, vol. 312, no. 5779, p. 1498, 2006.
[17] J. R. Friedman *et al.*, "Quantum superposition of distinct macroscopic states," *Nature*, vol. 406, pp. 43–46, 2000.
[18] J. Mooij and T. Orlando *et al.*, "Josephson persistent-current qubit," *Science*, vol. 285, p. 1036, 1999.